Reversibility of magnetic field driven transition from electronic phase separation state to single-phase state in manganites: A microscopic view

Hao Liu,[1] Lingfang Lin,[2] Yang Yu,[1] Hanxuan Lin,[1] Yinyan Zhu,[1] Tian Miao,[1] Yu Bai,[1] Qian Shi,[1] Peng Cai,[1] Yunfang Kou,[1] Fanli Lan,[1] Wenbin Wang,[1,3] Xiaodong Zhou,[1,3] Shuai Dong,[2,*] Lifeng Yin,[1,3,4,†] and Jian Shen[1,3,4,‡]

[1]*State Key Laboratory of Surface Physics and Department of Physics, Fudan University, Shanghai 200433, China*

[2]*School of Physics, Southeast University, Nanjing 211189, China*

[3]*Institute of Nanoelectronic Devices and Quantum Computing, Fudan University, Shanghai 200433, China*

[4]*Collaborative Innovation Center of Advanced Microstructures, Nanjing 210093, China*

(Received 16 July 2017; revised manuscript received 19 October 2017; published 27 November 2017)

Electronic phase separation (EPS) is a common phenomenon in strongly correlated oxides. For colossal magnetoresistive (CMR) manganites, the EPS is so pronounced that not only does it govern the CMR behavior, but also raises a question whether EPS exists as a ground state for systems or a metastable state. While it has been well known that a magnetic field can drive the transition of the EPS state into a single-phase state in manganites, the reversibility of this transition is not well studied. In this work we use magnetic force microscopy (MFM) to directly visualize the reversibility of the field driven transition between the EPS state and the single-phase state at different temperatures. The MFM images correspond well with the global magnetic and transport property measurements, uncovering the underlying mechanism of the field driven transition between the EPS state and the single-phase state. We argue that EPS state is a consequence of system quenching whose response to an external magnetic field is governed by a local energy landscape.

DOI: 10.1103/PhysRevB.96.195154

I. INTRODUCTION

Electronic phase separation (EPS) phenomena is widely found in many strongly correlated oxides where intricate interplay between spin, charge, orbital, and lattice degrees of freedom leads to various electronic phases with nearly degenerated energy [1–5]. Such degeneracy underlies rich phase diagrams of the systems as their ground states are particularly susceptible to small external perturbations. A microscopic and intrinsic electronic inhomogeneity is thus expected under certain conditions. One prominent example is perovskite manganites which show colossal magnetoresistance (CMR). In those manganites, EPS arises from phase competition between ferromagnetic metallic (FMM) phase and charged ordered insulating (COI) phases [6–10]. The COI phase is usually antiferromagnetic under zero magnetic field. Application of an external magnetic field tends to align the spins in the COI domains leading to the local first order transition from COI to FMM phase [9,11,12]. This magnetic field induced local melting of COI phase is generally considered to be the origin of CMR in manganites [13–17]. One salient character of this transition in a manganite system is its reversibility, as reflected in its strong thermal and magnetic hysteresis. Such reversibility revealed in macroscopic characterizations has to be correlated with a microscopic process in materials in which COI-to-FMM transition happens. It is thus vital to explore the transition at a microscopic scale. Understanding the reversibility of this transition is not only important to reveal the nature of the EPS state, but also important for future applications of CMR materials. Another intriguing aspect of this transition in manganites is its dynamic glassy behavior which shows nonergodicity and relaxation. Several experiments and theoretical calculations have argued that the first order COI-to-FMM transition is blocked under a glass freezing temperature leading to an EPS state. It is still an open question whether EPS exists as a ground state for systems or a metastable state due to such glass freezing. Therefore, the study of COI-to-FMM transition in manganites, especially its reversibility, will shed new light on the nature of EPS state. Its implications for glass physics also apply to a broad material class beyond manganites.

In this work we use a variable-temperature, high-field magnetic force microscope (MFM) [18–20] to investigate the reversibility of the COI-to-FMM transition in a model system of $(La_{2/3}Pr_{1/3})_{5/8}Ca_{3/8}MnO_3$ (LPCMO) thin films at a microscopic level. We note that previous MFM studies only follow the initial magnetization process [11,12,21]. The reversed process, i.e., whether the system would recover the initial state after the field is reduced, remains unknown. The LPCMO system is chosen because it consists of two competing FMM and COI phases forming an EPS state with a submicron length scale [22–26] that can be conveniently tracked by MFM. The obtained microscopic picture is then directly correlated with the global transport and magnetic properties, providing a comprehensive understanding of the energy competition among different electronic phases. Our experimental observations indicate that the field driven transition from the EPS state to the FMM state is irreversible at low temperatures. In other words, once the system has been transformed into an FMM single-phase state, it stays in the single-phase state even if the field is reduced to zero or swept to an opposite direction. However, at an intermediate temperature close to the global metal-insulator transition (MIT) point [$T_c \sim 100$ K in Fig. 2(a), see below], the transition between the EPS state and the FMM state becomes partially reversible with part of the melted COI domains recovering their COI state once the field is reduced to zero. At temperatures well above the MIT

*Corresponding author: sdong@seu.edu.cn
†lifengyin@fudan.edu.cn
‡shenj5494@fudan.edu.cn

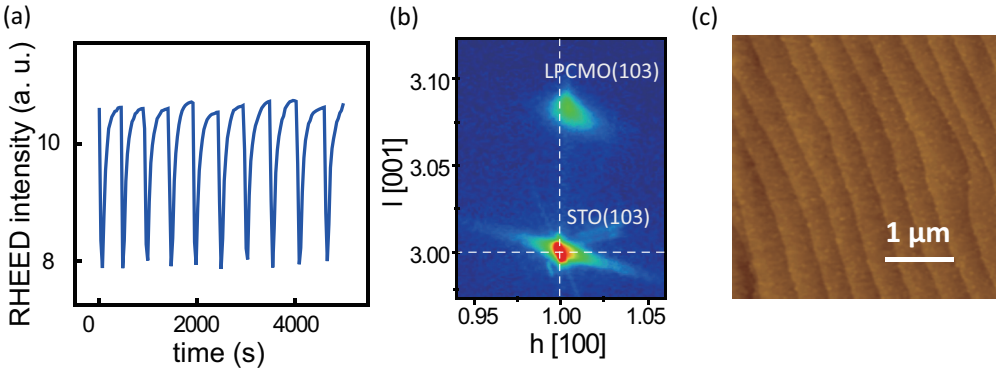

FIG. 1. (a) Unit cell by unit cell reflection high energy electron diffraction (RHEED) oscillations. (b) X-ray reciprocal space mapping (RSM) of the LPCMO thin film grown on STO(001). (c) Atomic force microscopic (AFM) image shows the morphology of the film.

point, the transition between the EPS state and the FMM state becomes fully reversible.

II. EXPERIMENTAL DETAILS

Epitaxial LPCMO thin films of 60 nm thickness were grown on titanium oxide terminated (001)-oriented $SrTiO_3$ (STO) substrates by a pulsed laser deposition system [27]. As shown in Fig. 1(a), the thin film growth is monitored by *in situ* reflection high energy electron diffraction (RHEED), whose unit cell by unit cell intensity oscillations indicate a good epitaxial thin film growth. The single crystallinity of the LPCMO films is confirmed by the sharp (r.u.l.) diffraction spot of the LPCMO thin film in an x-ray reciprocal map [Fig. 1(b)]. The slight off alignment between the diffraction spots of the film and substrate indicates that the film is partially strain relieved at 60 nm thickness. An atomic force microscopic image [Fig. 1(c)] shows a flat sample surface with clear atomic steps inherited from the substrate.

Figures 2(a) and 2(b) show the temperature-dependent resistivity (*R*-*T*) and magnetization (*M*-*T*) curves of the sample, respectively. The kink at 220 K (marked by a red arrow) in the *R*-*T* curve is known to be caused by the paramagnetic (PM)-to-COI transition ($T_{CO} \sim 220$ K), which also marks the onset of ferromagnetism as shown in the *M*-*T* curve. The FMM phase grows with decreasing temperature and forms the long range ferromagnetic order at 100 K ($T_c \sim 100$ K), as shown by the derivative peak of the *M*-*T* curve [inset of Fig. 2(b)]. The percolation of the FMM phase also leads to the insulator to metal transition at 100 K in the *R*-*T* curve. Figure 2(c) shows the magnetic anisotropy of the LPCMO films with both out-of-plane and in-plane magnetic hysteresis measured by a superconducting quantum interference device (SQUID). The hysteresis loops show that the easy magnetization axis of the thin films lies in the film plane which is attributed to the shape anisotropy of the thin films. To gain a microscopic view of the reversibility of the COI-to-FMM phase transition, MFM mapping was taken after the system was zero-field cooled down to three representative temperatures of 10, 80, and 160 K. Note that after MFM mapping was completed at each temperature, the system is warmed up to room temperature before being zero-field cooled to another selected temperature. For MFM imaging, both soft (coercivity ~100 Oe) and hard (coercivity ~1.3 T) magnetic tips have been used. The coercivity of the hard magnetic tips is larger than that of the LPCMO films, allowing us to flip the magnetization direction of the LPCMO films without changing the magnetization direction of the tips. As will be shown later, this is vital to

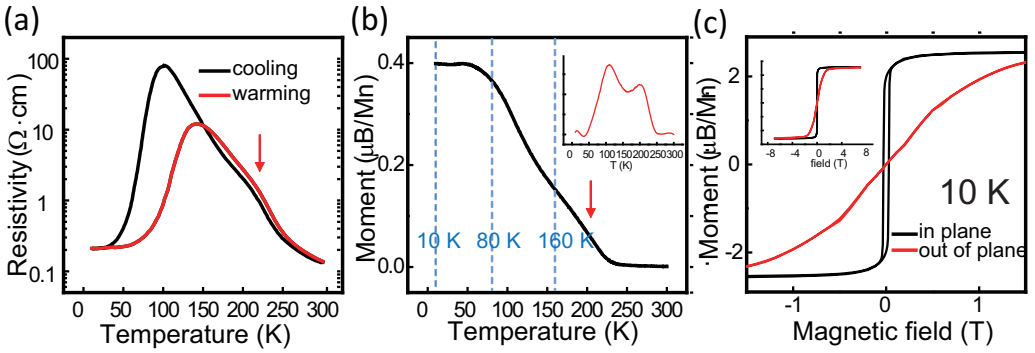

FIG. 2. (a) and (b) Temperature-dependent resistivity and magnetization curves, respectively. Resistivity was measured without applying any field and the hysteresis indicates the existence of phase separation in the film. Magnetization was acquired with a 1000 Oe in-plane magnetic field. The PM-to-COI and the COI-to-FM phase transition temperature are identified by the start of loop shoulder (220 K) and the peak (100 K) in the *R*-*T* curve cooling process, respectively. (c) Initial magnetization curves and *M*-*H* loops after zero-field cooling at 10 K. The magnetic field is applied out-of-plane (red line) and in-plane (black line). Red loop and black loop show typical ferromagnetic hard axis and easy axis loops, respectively.

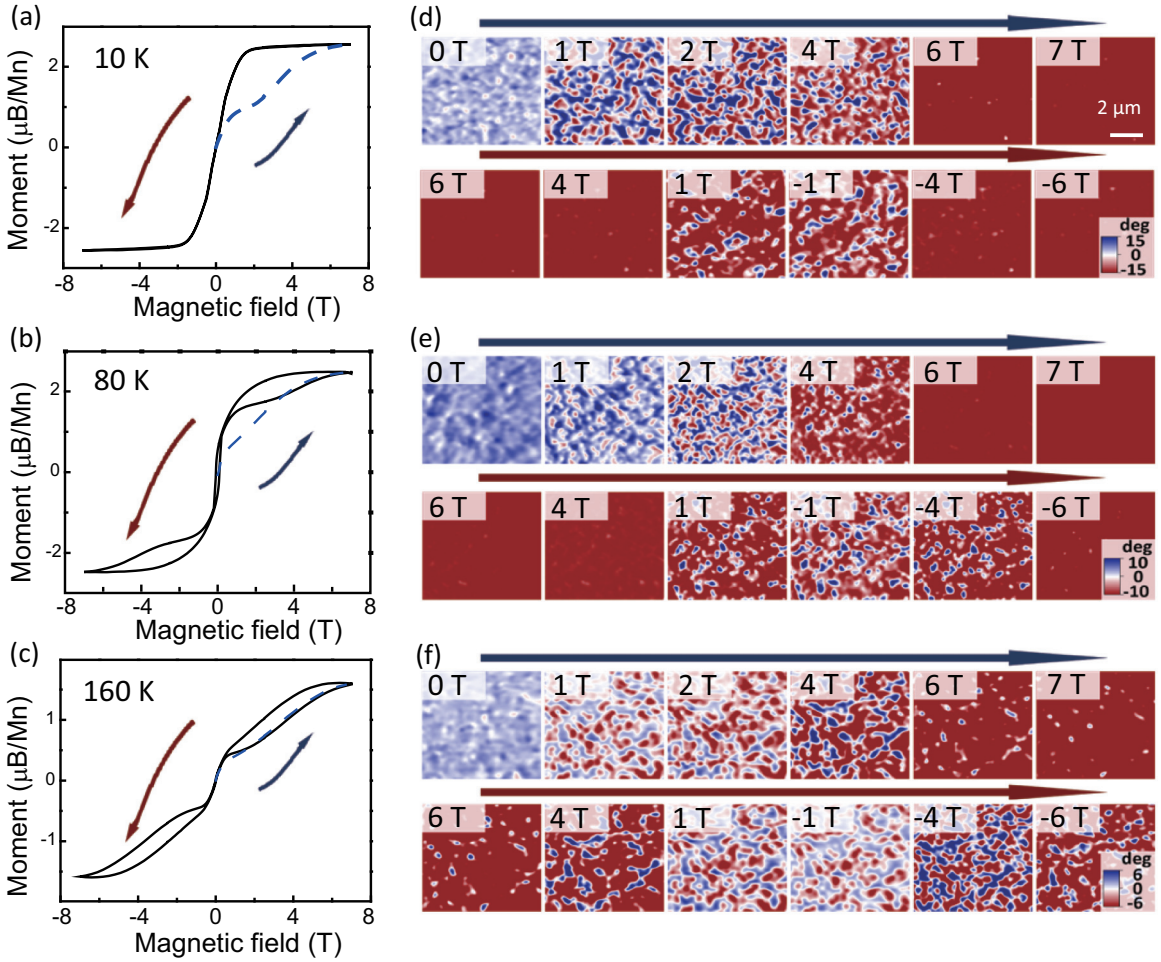

FIG. 3. (a)–(c) Initial magnetization curves (blue dashed lines) and *M-H* loops (black solid lines) measured at 10, 80, and 160 K, respectively. The MFM phase images (d)–(f) acquired with a soft magnetic tip at each selected temperature. MFM was conducted in a tapping mode in which the frequency was locked giving rise to phase deviation $\delta\varphi$ as a measured MFM signal. The scale bar in (d) is 2 μm and the color bar for (d)–(f) are $\pm$15, $\pm$10, and $\pm$6 deg. The blue and red arrows mark the initial process and field sweeping process from 7 to -7 T, respectively. All the MFM images were taken at almost the same zone which can be confirmed by the morphology.

distinguish MFM signals acquired from the nonferromagnetic COI domains and the oppositely oriented FMM domains.

Figures 3(a)–3(c) and 3(d)–3(f) show the global magnetization curves and MFM images measured at three representative temperatures (10, 80, and 160 K) with magnetic field applied perpendicular to the surface, respectively. Prior to measurements at each temperature, the system was warmed up to room temperature and subsequently cooled down to the selected temperature under zero field, allowing the system to stay in the virgin state before each measurement. Note the magnetization curves are measured along the magnetization hard axis in order to correlate with the MFM images which have to be taken with the field perpendicular to the surface. The blue dashed lines and the black solid lines are initial magnetization curves and subsequent magnetization curves, respectively. The post initial magnetization curves exhibit distinctly different features at the three selected temperatures. At 10 K, the post initial magnetization curve has no hysteresis representing a typical hard-axis behavior for a ferromagnetic system. At 80 K, the magnetization curve has an obvious hysteresis; however it is clearly different from a typical ferromagnetic hysteresis loop. At 160 K the unusual hysteresis behavior becomes even more pronounced.

The MFM images provide a microscopic view of the magnetic states for the system at the three selected temperatures. The MFM images in Fig. 3 were acquired using soft magnetic tips whose magnetization direction always follows the applied perpendicular field direction. In this case, the FMM domains with the magnetization component parallel to the external field provide an attractive force to the tips, which is represented in red in the MFM images. The domains without a parallel magnetization component are either in white (zero force) or blue (repulsive force to the tips). The blue is caused by the opposite magnetic flux of the stray field from the nearby FMM domain. For all three selected temperatures, the MFM images acquired during the initial magnetization process (marked by blue arrows) show explicitly the melting process of the COI phase, as indicated by the increase of the area fraction of the red FMM domains with increasing field. At 7 T, the system is in the single FMM state at 10 and 80 K and has only a tiny fraction of COI phase [white spots in Fig. 3(f)] at 160 K. When reducing the field from 7 to 0 T and subsequently increasing

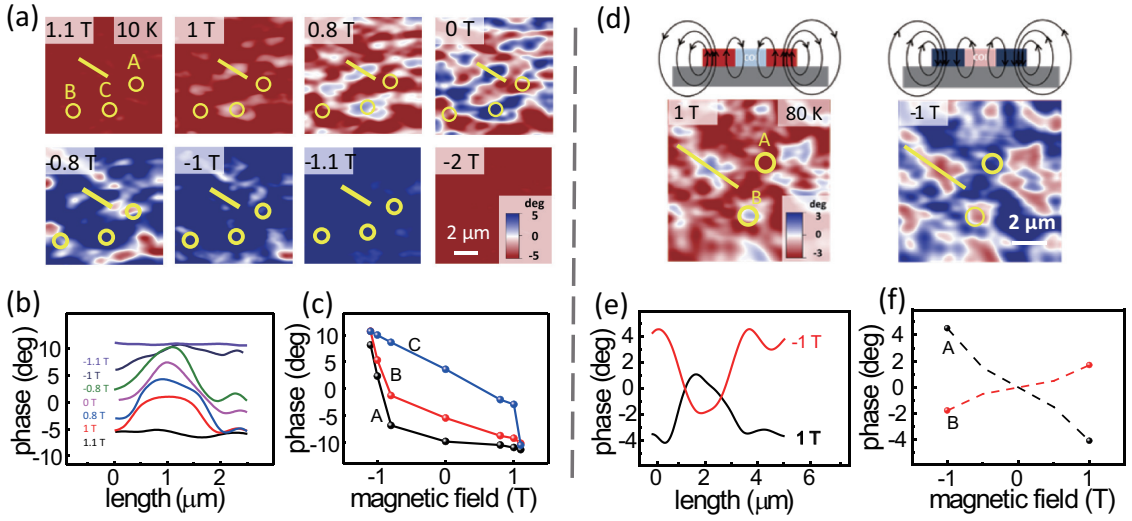

FIG. 4. (a) MFM phase images mapping with hard magnetic tip (coercivity ∼1.3 T) at 10 K after the initial melting process. The image series are chosen with the same process in Fig. 2. (d) Marked by blue arrow. Due to the stabilization of component in the hard magnetic tip, only the domain with antiparallel magnetization to the tip can give the dark blue color. (b) The line profile from the position marked by a white dashed line in (a). (c) The average MFM signal count at the selected position A B C. (d) MFM phase images mapping with hard magnetic tip at 80 K after the initial melting process. (e) and (f) The line profile and average MFM signal at the position marked by a dashed line and circle, respectively.

the field from 0 to −7 T (marked by red arrows), the blue regions reappear in field ranges of 1 to −1 T, 1 to −4 T, and 6 to −6 T at 10, 80, and 160 K, respectively. These blue regions can be either COI phase or FMM phase with magnetization direction opposite to that of the tip, or FMM phase with in-plane magnetization, all of which cannot be distinguished by the conventional soft magnetic tips used in Fig. 3. Note that some slight blue color can be seen in the sample's virgin state at 0 T because the closed flux from the in-plane FMM domains to the COI domains can still yield a small repulsive force to the tip. We also note that the shape of the EPS domains look almost isotropic indicating that the STO structural phase transition has no significant effect on the EPS domain, which otherwise will lead to some preferred alignment along certain crystallographic axes.

To understand the nature of the blue regions, we use hard magnetic tips (coercivity is ∼1.3 T) [28] in the MFM setup to image the samples. A 9 T a perpendicular field was first applied to the system during the initial magnetization process, which is high enough to align the magnetization of the sample and the tip along the field direction. The field is then reduced to 0 T and subsequently increased from 0 to −2 T in the opposite direction. Figure 4(a) shows MFM images acquired with field changing from 1.1 to −2 T in this process at 10 K. Before the field is increased beyond −1.3 T, the magnetization direction of the tip remains in its original direction due to its large coercivity. With changing field from 1.1 to −1.1 T, the nucleation and growth of the blue domains can be clearly seen in the MFM images. The area fraction of the blue regions increases monotonically till full coverage and no blue regions are observed to turn back into red. This indicates that all regions are ferromagnetic because the nonferromagnetic COI regions should exhibit red due to flux closure from the neighboring ferromagnetic regions. The MFM signal line profiles of the marked lines [Fig. 4(b)] and the average MFM signal of the marked circle regions [Fig. 4(c)] indicate that the MFM signals obtained at the same surface locations at 1.1 and −1.1 T have the same amplitude but opposite sign. This further proves that the blue regions are FMM phase with opposite magnetization with respect to that of the red FMM regions. Not surprisingly, when the field reaches −2 T, all regions turn red because the tip magnetization direction is reversed by the field. We thus conclude that at 10 K the COI phase cannot be recovered once melted into the FMM phase by the magnetic field, and consequently the field driven transition of the EPS state into a single FMM state is irreversible. The situation becomes quite different at 80 K. Figure 4(d) shows the MFM images acquired at 1 and −1 T using the hard magnetic tip after an initial magnetization process at 80 K. Figures 4(e) and 4(f) show the MFM signal line profiles of the marked lines and the average MFM signal of the marked circle regions in Fig. 4(d). While the two images were obtained by the same tip with the same magnetization direction, the domains in the two images exhibit MFM signals with opposite signs. Considering the fact that ferromagnetic domains tend to switch its magnetization direction following the direction of the external field, it is obvious that those domains with red color in the −1 T image are not FMM domains which otherwise should not switch to antiparallel direction with respect to that of the field. This means that the corresponding domains in the 1 T image are reappeared COI domains when the field is decreased from 7 to 1 T. In other words, at 80 K the field driven transition from the EPS state to the single FMM state is partially reversible. At 160 K, the COI phase is energetically more favorable and cannot be fully melted even under 7 T field [Fig. 3(f)]. Consequently, the initial magnetization curve is fully overlapped with the magnetization hysteresis curve [Fig. 3(c)]. While there are certainly domain walls between

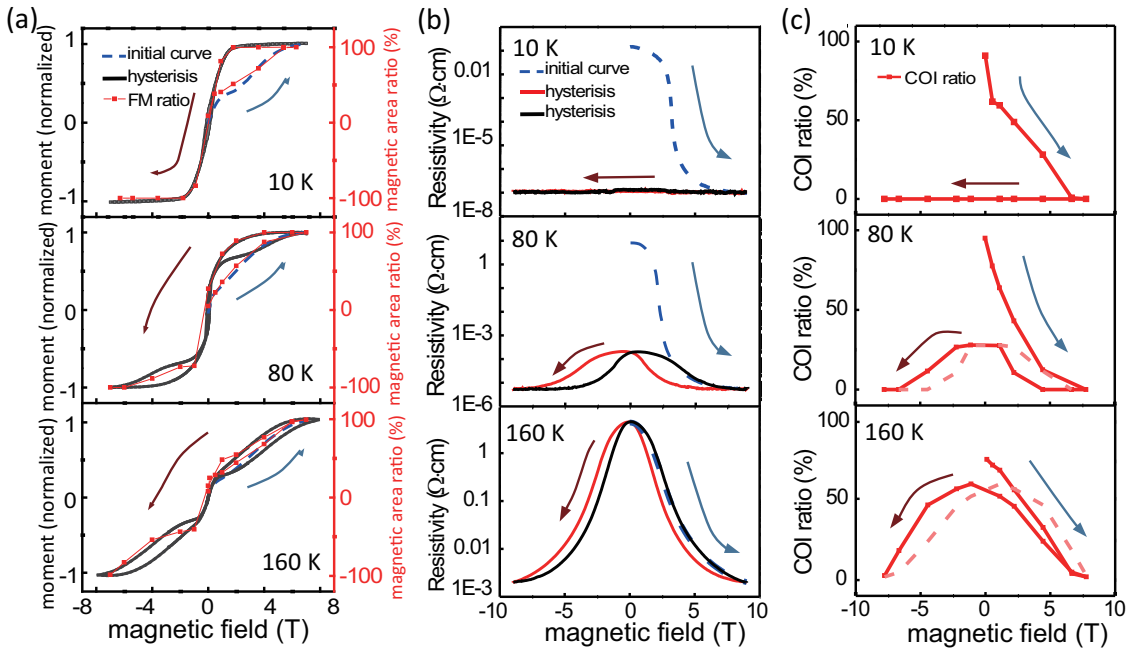

FIG. 5. (a) Initial magnetization curves and *M-H* loops compared with FM domain ratio (from MFM images) curves at temperature of 10 K, 80 K, and 160 K, respectively. The sample was cooled from room temperature to low temperature without magnetic field. At the beginning of each curve, the phase separation state is the dominant ground state. (b) Magnetic-field-dependent resistivity curves measured at selected temperature. (c) The COI (blue and white pattern in Figs. 3(d)–3(f)) area ratio vs magnetic field curves. All of the curves include an initial melting process and a magnetic field swapping process. To show the hysteresis, mirrored curves of the data from 7 T to −7 T are given in (c) by dashed light red curves just for guiding the eyes.

two FMM domains or FMM-COI domains, we can only identify their positions as white stripes in Figs. 4(a) and 4(d) whose internal magnetic structure is beyond our MFM spatial resolution.

Having known how FMM and COI domains evolve under magnetic field, we can establish a direct correlation between the macroscopic properties of the system with the evolution of microscopic domain patterns. Figure 5(a) show the field-dependent area fraction of FMM domains (red dots) deduced from the MFM images for the three selected temperatures. The MFM data points match very well with the global magnetization measurements of the sample (black solid lines and blue dashed lines). The hysteretic behavior of the hard-axis magnetization curves at 80 and 160 K is caused by the partial or full reversibility of the field induced transition from EPS to a single-phase state. At these temperatures, the COI phase reappears once the field is reduced to zero and is subsequently remelted by the opposite external magnetic field, giving rise to the unusual hysteretic behavior. In contrast, at 10 K the hard-axis magnetization curve has no hysteresis because the system stays in the FMM state once transited from the EPS state by the field.

Figures 5(b) and 5(c) show the field-dependent resistivity curves (left column) and the area fraction of the COI phase deduced from the MFM images in Fig. 3 (right column). Prior to the initial magnetization, the system is dominated by the COI phase and has the maximum resistivity. With increasing field during the initial magnetization process, the COI phase is melted and its area fraction decreases accordingly. When the area fraction of the COI phase is reduced to 50%, the global resistivity drops rapidly reflecting the percolation of the FMM domains [27,29]. At 10 K after the initial magnetization process is completed, all the COI domains are melted to become FMM phase and this process is irreversible. We note that the irreversible transition from the EPS state to a single FMM state is useful when the half-metallic LPCMO system is applied as magnetic electrodes in spintronic devices. At 80 K, the transition from the EPS state to the FMM state is partially reversible. The area fraction of the reappeared COI domains reaches ∼30% from 2 to −2 T. The field-dependent resistivity behavior closely resembles that of the field-dependent area fraction of the COI phase. At 160 K, the COI phase dominates. The transition from the EPS state to the FMM state is almost fully reversible. This gives a large magnetoresistance over 10^5%.

III. SIMULATION AND DISCUSSION

To help the understanding of our experimental observations, we carry out the random-field Ising model (RFIM) simulation [23] via Monte Carlo method. Despite the simplicity, the RFIM has been proved to give a successful phenomenological description of large scale EPS in manganites [2,23,30,31]. The typical simulation results are show in Fig. 6 in which the red (blue) region represents FMM (COI) phase. We carefully choose the starting FMM/COI area ratio to represent our experimental situations at 10, 80, and 160 K [see Figs. 3(d)–3(f)]. For all cases, the COI phase can be melted into FMM phase by increasing the external magnetic field parametrized as h here. The quantitative difference occurs

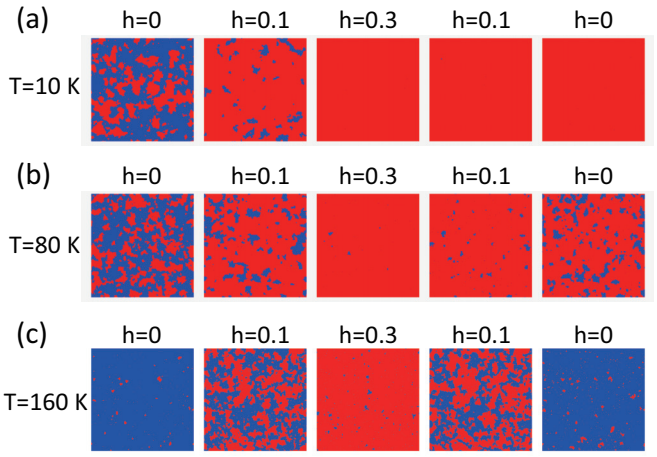

FIG. 6. Numerical simulation of the EPS patterns as a function of external magnetic field. (a) Low temperature case. (b) Intermediate temperature case. (c) High temperature case. The FMM and COI regions are denoted by red and blue, respectively.

when the magnetic field is reduced to zero. For the low temperature case, the field driven transition from EPS to FMM is almost irreversible even when the external magnetic field is removed. In contrast, for the high temperature case, this transition is fully reversible to COI after the removal of the magnetic field. At intermediate temperature, the transition is partially reversible with FMM volume increased. These simulated results agree with experimental observation quite well, implying our simplified model has captured the main physics in the phenomenological level.

Based on our experimental observation and model simulation, we now discuss the nature of the EPS state in manganites. It has been intensively debated whether EPS in manganites should be treated as a ground state or a metastable state in a process of COI-to-FMM transition. The latter thought argues that glass freezing blocks the COI-to-FMM transition in the middle stage leading to the EPS state at low temperatures. The reversibility of the COI-to-FMM transition we study here is closely related to such glass physics. First, the dependence of the field history of the EPS state implies that the EPS pattern is determined by the local minima of the energy landscape, instead of the "global" minimum of energy. In other words, even in the FMM preferred region (the low temperature case here), the system can be locally trapped to the COI phase to form the EPS state. An external magnetic field can help the COI part to overcome the energy barriers between local minima and reach a lower energy valley close to the full FMM limit. Then this energy valley is low enough to be stable after the removal of the magnetic field. In addition, the low temperature can also suppress the energy excitation and help the freezing of FMM state. In contrast, for the COI preferred region (the high temperature case here), the FMM state is much higher in free energy, which can only be stabilized by a large external magnetic field. After the removal of the magnetic field, the COI state is fully reversible with the help of a large thermal fluctuation. In the middle region (the intermediate temperature here), the close energies between the FMM and the COI phase generate many local minima of the energy landscape. Then after the removal of the magnetic field, the system can be easily trapped in a metastable energy valley close to the full FMM limit, resulting in partial reversibility.

IV. SUMMARY

In conclusion, we have investigated the temperature-dependent reversibility of the field driven transition from the EPS state to the single FMM state in the LPCMO system. At low temperatures, the transition is irreversible. At temperatures near T_c where the competing FMM and COI phases are closest in energy, the transition becomes partially reversible. At high temperatures near T_{CO}, the COI phase is energetically favorable and the transition is fully reversible. The nearly perfect match between the global physical properties and the microscopic domain evolution indicates that the physical properties of the system are dominated by evolution of the EPS state in the system whose response to the external magnetic field is governed by the local energy landscape. Our observation is also highly valuable for the application of manganite materials in spintronics as it gives clear guidance on how to achieve EPS state or single FMM state by design.

ACKNOWLEDGMENTS

This work was supported by National Key Research and Development Program of China (Grants No. 2016YFA0300701 and No. 2016YFA0300702), National Basic Research Program of China (973 Program) (Grant No. 2014CB921104); National Natural Science Foundation of China (Grant No. 11504053); Shanghai Municipal Natural Science Foundation (Grants No. 14JC1400500, No. 17ZR1442400, and No. 17ZR1442600); China Postdoctoral Science Foundation (Grants No. 2017M610221, No. KLH1512080, and No. KLH1512089); Shanghai Sailing Program (Grant No. 17YF1429000) and the National Postdoctoral Program for Innovative Talents.

[1] E. Dagotto, Science **309**, 257 (2005).
[2] E. Dagotto, T. Hotta, and A. Moreo, Phys. Rep. **344**, 1 (2001).
[3] N. Mathur and P. Littlewood, Phys. Today **56**(1), 25 (2003).
[4] K. H. Ahn, T. Lookman, and A. R. Bishop, Nature (London) **428**, 401 (2004).
[5] G. C. Milward, M. J. Calderon, and P. B. Littlewood, Nature (London) **433**, 607 (2005).
[6] M. H. Burkhardt, M. A. Hossain, S. Sarkar, Y.-D. Chuang, A. G. Cruz Gonzalez, A. Doran, A. Scholl, A. T. Young, N. Tahir, Y. J. Choi, S.-W. Cheong, H. A. Dürr, and J. Stöhr, Phys. Rev. Lett. **108**, 237202 (2012).
[7] C. Sen, G. Alvarez, and E. Dagotto, Phys. Rev. Lett. **98**, 127202 (2007).
[8] Y. Tokura, Rep. Prog. Phys. **69**, 797 (2006).
[9] W. Kundhikanjana, Z. Sheng, Y. Yang, K. Lai, E. Y. Ma, Y.-T. Cui, M. A. Kelly, M. Nakamura, M. Kawasaki, Y. Tokura, Q. C.

Tang, K. Zhang, X. X. Li, and Z.-X. Shen, Phys. Rev. Lett. **115**, 265701 (2015).
[10] J. Tao, D. Niebieskikwiat, M. Varela, W. Luo, M. A. Schofield, Y. Zhu, M. B. Salamon, J. M. Zuo, S. T. Pantelides, and S. J. Pennycook, Phys. Rev. Lett. **103**, 097202 (2009).
[11] W. D. Wu, C. Israel, N. Hur, S. Park, S. W. Cheong, and A. De Lozanne, Nat. Mater. **5**, 881 (2006).
[12] H. B. Zhou, L. F. Wang, Y. B. Hou, Z. Huang, Q. Y. Lu, and W. B. Wu, Nat. Commun. **6**, 8980 (2015).
[13] H. Kuwahara, Y. Tomioka, A. Asamitsu, Y. Moritomo, and Y. Tokura, Science **270**, 961 (1995).
[14] Y. Tomioka, A. Asamitsu, H. Kuwahara, Y. Moritomo, and Y. Tokura, Phys. Rev. B **53**, R1689 (1996).
[15] T. Z. Ward, S. Liang, K. Fuchigami, L. F. Yin, E. Dagotto, E. W. Plummer, and J. Shen, Phys. Rev. Lett. **100**, 247204 (2008).
[16] Y. Tokura, Y. Tomioka, H. Kuwahara, A. Asamitsu, Y. Moritomo, and M. Kasai, Physica C **263**, 544 (1996).
[17] H. Y. Zhai, J. X. Ma, D. T. Gillaspie, X. G. Zhang, T. Z. Ward, E. W. Plummer, and J. Shen, Phys. Rev. Lett. **97**, 167201 (2006).
[18] K. Du, K. Zhang, S. Dong, W. G. Wei, J. Shao, J. B. Niu, J. J. Chen, Y. Y. Zhu, H. X. Lin, X. L. Yin, S. H. Liou, L. F. Yin, and J. Shen, Nat. Commun. **6**, 6179 (2015).
[19] D. Rugar, H. J. Mamin, P. Guethner, S. E. Lambert, J. E. Stern, I. McFadyen, and T. Yogi, J. Appl. Phys. **68**, 1169 (1990).
[20] L. W. Zhang, C. Israel, A. Biswas, R. L. Greene, and A. de Lozanne, Science **298**, 805 (2002).
[21] Y. Murakami, H. Kasai, J. J. Kim, S. Mamishin, D. Shindo, S. Mori, and A. Tonomura, Nat. Nanotechnol. **5**, 37 (2010).
[22] P. Littlewood, Nature (London) **399**, 529 (1999).
[23] A. Moreo, M. Mayr, A. Feiguin, S. Yunoki, and E. Dagotto, Phys. Rev. Lett. **84**, 5568 (2000).
[24] P. G. Radaelli, R. M. Ibberson, D. N. Argyriou, H. Casalta, K. H. Andersen, S. W. Cheong, and J. F. Mitchell, Phys. Rev. B **63**, 172419 (2001).
[25] L. Ghivelder and F. Parisi, Phys. Rev. B **71**, 184425 (2005).
[26] M. Uehara, S. Mori, C. H. Chen, and S. W. Cheong, Nature (London) **399**, 560 (1999).
[27] W. G. Wei, Y. Y. Zhu, Y. Bai, H. Liu, K. Du, K. Zhang, Y. F. Kou, J. Shao, W. B. Wang, D. L. Hou, S. Dong, L. F. Yin, and J. Shen, Phys. Rev. B **93**, 035111 (2016).
[28] S. H. Liou and Y. D. Yao, J. Magn. Magn. Mater. **190**, 130 (1998).
[29] S. Dong, H. Zhu, X. Wu, and J.-M. Liu, Appl. Phys. Lett. **86**, 022501 (2005).
[30] See Supplemental Material at http://link.aps.org/supplemental/10.1103/PhysRevB.96.195154 for the description of RFIM simulation.
[31] Y. Y. Zhu, K. Du, J. B. Niu, L. F. Lin, W. G. Wei, H. Liu, H. X. Lin, K. Zhang, T. Y. Yang, Y. F. Kou, J. Shao, X. Y. Gao, X. S. Xu, X. S. Wu, S. Dong, L. F. Yin, and J. Shen, Nat. Commun. **7**, 11260 (2016).